Dielectric response of BaTiO$_3$ electronic states under AC fields via microsecond time-resolved X-ray absorption spectroscopy

S. Kato [a,*], N. Nakajima [a], S. Yasui [b,c], S. Yasuhara [b,d], D. Fu [e,f,g], J. Adachi [h], H. Nitani [h], Y. Takeichi [h], A. Anspoks [i]

[a] *Graduate School of Advanced Science and Engineering, Hiroshima University, 1-3-1 Kagamiyama, Higashihiroshima, Hiroshima 739-8562, Japan*
[b] *Laboratory for Materials and Structures, Tokyo Institute of Technology, 4259-J2-19 Nagatsuta-cho, Midori-ku, Yokohama 226-8503, Japan*
[c] *Laboratory for Advanced Nuclear Energy, Tokyo Institute of Technology, 2-12-1 N1-16 Ookayama, Meguro-ku, Tokyo 152-8550, Japan*
[d] *School of Materials and Chemical Technology, Tokyo Institute of Technology, 2-12-1 Ookayama, Meguro-ku, Tokyo 152-8550, Japan*
[e] *Department of Electronics and Materials Science, Faculty of Engineering, Shizuoka University, 3-5-1 Johoku, Naka-ku, Hamamatsu 432-8561, Japan*
[f] *Department of Engineering, Graduate School of Integrated Science and Technology, Shizuoka University, 3-5-1 Johoku, Naka-ku, Hamamatsu 432-8561, Japan*
[g] *Department of Optoelectronics and Nanostructure Science, Graduate School of Science and Technology, Shizuoka University, 3-5-1 Johoku, Naka-ku, Hamamatsu 432-8561, Japan*
[h] *Institute of Materials Structure Science, High Energy Accelerator Research Organization (KEK), 1-1 Oho, Tsukuba, Ibaraki 305-0801, Japan*
[i] *Institute of Solid State Physics, University of Latvia, Kengaraga street 8, Riga, LV-1063, Latvia*

ARTICLE INFO

ABSTRACT

For the first time, the dielectric response of a BaTiO$_3$ thin film under an AC electric field is investigated using microsecond time-resolved X-ray absorption spectroscopy at the Ti K-edge in order to clarify correlated contributions of each constituent atom on the electronic states. Intensities of the pre-edge e_g peak and shoulder structure just below the main edge increase with an increase in the amplitude of the applied electric field, whereas that of the main peak decreases in an opposite manner. Based on the multiple scattering theory, the increase and decrease of the e_g and main peaks are simulated for different Ti off-center displacements. Our results indicate that these spectral features reflect the inter- and intra-atomic hybridization of Ti 3d with O 2p and Ti 4p, respectively. In contrast, the shoulder structure is not affected by changes in the Ti off-center displacement but is susceptible to the effect of the corner site Ba ions. This is the first experimental verification of electronic contribution of Ba to polarization reversal.

1. Introduction

Ferroelectric materials are widely used in various practical applications, including in multilayer ceramic capacitors, actuators, and memory cells, among others. However, to understand the dielectric response of these materials, it is essential to first understand the dynamic behavior of spontaneous polarization reversal under an electric field. Among ferroelectric materials, perovskite titanates (ATiO$_3$; A=Pb, Ba, Sr, Ca) attract significant attention owing to the versatility of the functional solid solutions that are composed from them. In particular, a lack of space-inversion symmetry is a prerequisite for the occurrence of spontaneous polarization; therefore, previous related literature is primarily focused on the crystal structure. In the case of perovskite titanates, the off-center displacement of Ti ions in the TiO$_6$ octahedra is a major cause of polarization. [1–6] Various studies have been performed to study X-ray absorption of Ti K-edge for BaTiO$_3$. [7–11]

Furthermore, it is obvious that also A-site cations significantly affect dielectric properties of ATiO$_3$, including magnitude of polarization and Curie temperature. [12–14] Cohen was the first to theoretically demonstrate the existence of Pb 6s and O 2p hybridization in PbTiO$_3$, [15] going beyond the hard-sphere model. This prediction was experimentally verified by Kuroiwa *et al.* via high-precision X-ray diffraction analysis, which revealed the electron density distribution between Pb and apical O. [16] Recently, Anspoks *et al.* reported the correlation effects of A-site ions in O and Ti based on the reverse Monte Carlo method applied to the extended X-ray absorption fine structure (EXAFS) data. [17]

Thus, it is quite evident that orbital hybridization between constituent atoms is closely linked to the dielectric properties of ATiO$_3$. Hence, direct observation of the electronic states under the

---

* Corresponding author.
E-mail address: kato-seiya@hiroshima-u.ac.jp (S. Kato).

application of an electric field is an appropriate approach to investigate the dielectric properties of ferroelectric materials. We employed microsecond time-resolved (TR) X-ray absorption spectroscopy (XAS) because tiny changes in spectra are expected by the previous studies. [18,19] The TR measurement is essential to exclude any undesired influences caused by a DC measurement such as Joule heating and fatigues. In this study, we selected BaTiO$_3$ as the target material whose electronic states at the instant of polarization reversal were observed via microsecond TR-XAS measurements. XAS is an element-specific technique, which is sensitive to local bonding around absorbing atoms. Combined with the TR approach, XAS can be used for the investigation of the polarization reversal response of the atomic bonds in BaTiO$_3$.

In particular, in this study, TR-XAS data of BaTiO$_3$ at the Ti K-edge are used to investigate the response of the corresponding electronic states under an applied AC electric field. It was observed that intensities of the pre-edge e_g peak and shoulder structure just below the main edge increase as the electric polarization increases, whereas that of the main peak decreases in an opposite manner. This observation indicates that in addition to Ti 3d-O 2p hybridization, a correlated effect of Ba ions on Ti electronic states also contributes to polarization reversal in BaTiO$_3$.

2. Experimental

An epitaxial BaTiO$_3$(001) film with a thickness of 650 nm was prepared using pulsed laser deposition on a 0.5 mm thick (LaAlO$_3$)$_{0.3}$-(SrAl$_{0.5}$Ta$_{0.5}$O$_3$)$_{0.7}$(001) substrate along with a 100 nm thick SrRuO$_3$(001) buffer layer, which also acted as the bottom electrode. A 50 nm Pt with a diameter of 100 μm was evaporated on the BaTiO$_3$ film, which acted as the top electrode. Film growth was verified via X-ray diffraction as shown in Fig. 1. It was confirmed that all layers had a preferred (001) orientation normal to the surface of the film. In addition, the lattice constant, c, of the BaTiO$_3$ film calculated based on the (002) peak was 4.136 Å, which is longer than that of the standard powder ($c = 4.018$ Å). [12] This lattice mismatch between the BaTiO$_3$ film and substrate induces a compressive strain. [20] The preferred orientation of c-axis is also reported in thin films with SrTiO$_3$ substrates where misfit strain is smaller than our sample. [21] This result guarantees that the influence of a domain and the domain wall motion under electric fields are negligible in our case.

The ferroelectricity of the film was verified by measuring polarization-electric field ($P − E$) hysteresis using a ferroelectric tester (Toyo Corporation, FCE-fast) with a triangular electric field of 1 kHz; these results are shown in Fig. 2. The open loops indicate ferroelectricity of the film both before (solid) and after (dot-
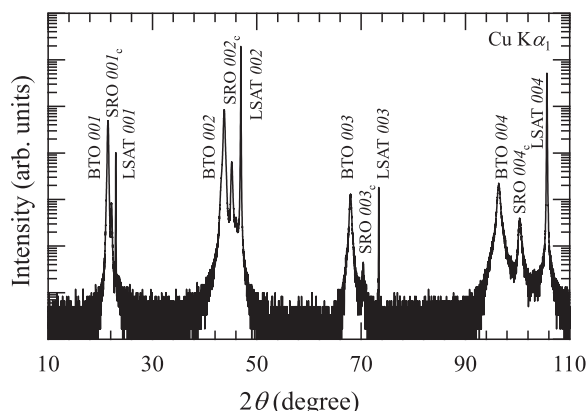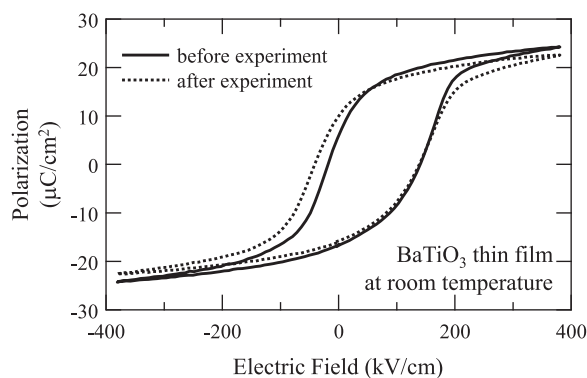

Fig. 2. $P − E$ hysteresis loops of the BaTiO$_3$ thin film before (solid) and after (dotted) TR-XAS measurements.
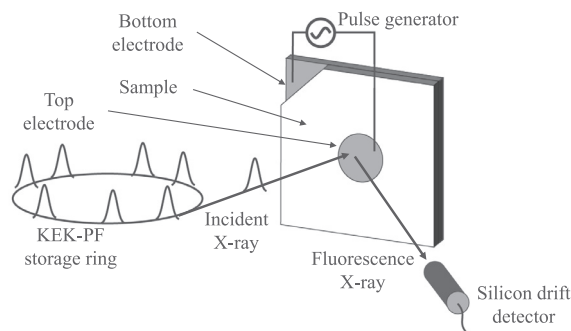

Fig. 3. Schematic diagram of the TR-XAS experimental setup.

ted) TR-XAS measurements. These loops are shifted in the positive electric field direction indicating a preferred downward polarization. [22,23] This imprint effect is due to the extrinsic interface effect, including the asymmetric properties of the top and bottom electrodes. [24] It should be noted that whereas the saturation polarization decreased, the magnitude of the negative coercive field increased after the TR-XAS measurements; these observations might be attributed to the fatigue effects caused by domain pinning and microcracking; [25] however, the dielectric properties of the sample remain even after experiments because hysteresis loop is closed as shown in Fig. 2, indicating low leakage current density. The currents at the maximum voltage before and after the TR-XAS measurements were 1.1 μA and 1.2 μA, respectively. The difference is below the experimental error, therefore it does not produce any detectable change in the TR-XAS data.

XAS experiments were performed on the beamline BL-15A1 equipment at the Photon Factory of the High Energy Research Organization (KEK-PF) using a Si (111) liquid-nitrogen cooled double-crystal monochromator. The X-ray beam was focused to 20 μm(H) × 20 μm(V) at the sample, which ensured the inclusion of the entire beam on a top electrode. Ti K-edge spectra were recorded in partial fluorescence yield mode using a Si drift detector (SDD), as illustrated in the schematic diagram shown in Fig. 3. X-rays were incident on the top electrode of the film at an angle of 45° from the surface normal. Furthermore, the detected X-rays were converted to digital signals using a digital signal processor (DSP; Techno-AP, APU101) with the addition of a time stamp for each signal.

TR-XAS measurements were realized using the time-stamp information based on the step-scan method. Fig. 4 shows the block diagram of the signal processing system employed in this study. The internal time of the DSP was repeatedly reset to 0 every 3 ms using a clear pulse generated by a delayed pulse generator (SRS,
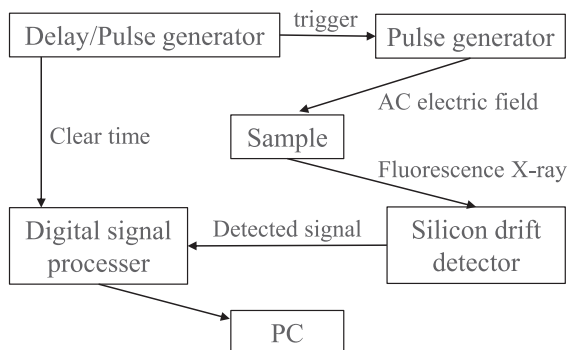

Fig. 1. X-ray diffraction pattern of the BaTiO$_3$(001) thin film grown on a SrRuO$_3$(001)/(LaAlO$_3$)$_{0.3}$-(SrAl$_{0.5}$Ta$_{0.5}$O$_3$)$_{0.7}$(001) substrate.

Fig. 4. Block diagram of the signal processing system synchronized with the applied voltage.

DG645). In addition, the same clear pulse was also input into the wave generator as a trigger pulse to apply the electric field to the film. In particular, one cycle of the applied voltage consisted of a single triangular pulse (±25 V, 1 kHz) and null voltage for 2 ms. Using this cycle, it was possible to assign a timing to the detected X-ray signals in response to the applied voltage, thereby enabling TR measurements. Several scans were summed to obtain the final Ti K-edge spectra with sufficient statistics. Because TR-XAS measurements require a long duration—e.g., 8 h for one spectral region— we focused on only three spectral features in our study, namely e_g peak, shoulder structure, and main peak.

3. Results & Discussion

A non-TR Ti K-edge spectrum of the BaTiO$_3$ thin film is shown in Fig. 5, along with that of standard BaTiO$_3$ powder as a reference. The absorption profile above the sharp main peak at 4985 eV corresponds to the density of states of the unoccupied Ti 4p states, whereas small features in the pre-edge region (4965–4975 eV) represent the Ti 3d states. In the case of an octahedral symmetry, the five-fold degenerate 3d orbitals split into three-fold and two-fold degenerate states with t_{2g} and e_g symmetries, respectively. A tiny hump at 4967 eV corresponds to the t_{2g} peak, whereas clear peaks at 4969 eV can be attributed to e_g. The reason why t_{2g} peak intensity is very weak is mainly because it is forbidden in a dipole and is allowed in quadrupole approximation. In the K-edge spectra, the probability of the 1s to 3d transition is much lower than that of the dipole transition. This effect can be observed in other bulk materials. [26,27] The intensity of the e_g peak increases as the local distortion in the TiO$_6$ octahedron increases, because the $pd\sigma$ hybridization between the Ti-3d e_g orbitals and O $p\sigma$ orbitals be-
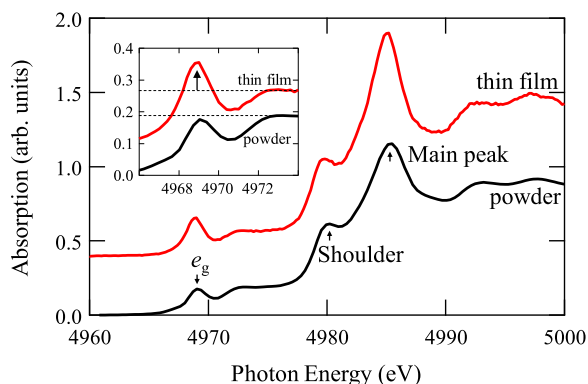

Fig. 5. Ti K-edge X-ray absorption near-edge spectra for a BaTiO$_3$ thin film and standard powder at room temperature.

comes more pronounced, resulting in a relatively large dipole component. It has been reported that the intensity of the e_g peak is proportional to the mean-square displacement of a Ti ion from the center of the TiO$_6$ octahedron. [26,28]

As shown in the inset of Fig. 5, the e_g peak of the BaTiO$_3$ thin film is larger than that of standard powder. In addition, the t_{2g} hump of the thin film almost flattens out. This observation can be attributed to the compressive strain resulting from the lattice mismatch between the BaTiO$_3$ film and underlying substrate. Because the BaTiO$_3$ film has a preferred orientation of the c-axis with enhanced tetragonality, a distinct dielectric response can be expected.

The shoulder structure at 4980 eV is a characteristic of BaTiO$_3$. Though the electronic states responsible for this structure have not been identified yet, the shoulder structure indicates the contribution of the A-site ions in the ferroelectric perovskite ATiO$_3$; the room-temperature spectra of commercial ATiO$_3$ powders (A = Pb, Ba, and Sr) are shown in Fig. 6(a). XAS technique is sensitive to the symmetry and electronic states. As the electronic states differ according to the chemical composition, so do the absorption spectra. For example, the Ti-K edge spectra of TiO, Ti$_2$O$_3$, and TiO$_2$ (anatase, rutile, and brookite) shown in Fig. 6(b) are different because their electronic states such as band structures are completely different.

In contrast to paraelectric SrTiO$_3$ with the cubic symmetry for which no shoulder structure is observed in its spectra, ferroelectric BaTiO$_3$ and PbTiO$_3$ with the tetragonal symmetry do exhibit shoulder structures. Differences in near edge structure between BaTiO$_3$ and PbTiO$_3$ may be due to differences in the hybridization of Ti 4p states with the states of A-site ions (i.e., Ba 6p vs Pb 6p). [29] Moreover, the intensity of these structures seems to depend on the degree of ferroelectricity; accordingly, PbTiO$_3$ has a more prominent shoulder structure compared with BaTiO$_3$.

This trend can also be confirmed based on a series of Ti K-edge spectra of Ba$_{1-x}$Ca$_x$TiO$_3$ (x = 0, 0.1, 0.18, 0.233, and 0.3), which are shown in Fig. 7. In particular, Ba$_{1-x}$Ca$_x$TiO$_3$ stays in the tetragonal phase within the considered x range, and therefore, ferroelectricity remains stable. [30,31] As can be seen in Fig. 7, the intensity of the shoulder structure decreases monotonically with increasing x, i.e., decreasing Ba concentration. Similar results have been reported for BaTi$_{1-x}$Zr$_x$O$_3$. [32,33] Likewise, the intensity of the shoulder structure decreases with an increase in x, i.e., decrease in the Ti content. From these results, it can be concluded that the intensity of the shoulder structure in the BaTiO$_3$ spectra reflects the electronic hybridization between Ti and Ba. This seemingly implausible claim has a theoretical background proposed by Ghosez et al. based on the Born effective charges of each constituent atom. [34]

As discussed above, because the e_g peak and shoulder structure directly reflect the ferroelectricity of perovskite titanates, we focused on these structures as well as the main peak in our TR experiments. The time variation of the applied electric field (E) for one cycle is shown in Fig. 9(d); a symmetric positive-and-negative triangular field for 1 ms and a field-free duration time for 1 ms were applied in sequence. The time variation of the triangular pulse corresponds to 1 kHz, which is the same frequency as that used for the hysteresis measurements. It should be noted that the field-free region is included to prevent Joule heating as well as to provide the field-free condition. In addition, we utilized not static but AC electric field to eliminate any undesired influence from fatigue, which ensures that the relative change in a short time frame is detectable. We have not observed any measurable drift of the observed values upon time.

The maximum variation of spectra with electric fields is shown in Fig. 8. The increase of e_g peak intensity is 0.6 % and the peak shifts are not observed. These tiny changes are due to a small distortion caused by electric fields. [18,19] The unchanged Ti oxidation state before and after experiments is verified by seeing peak posi-
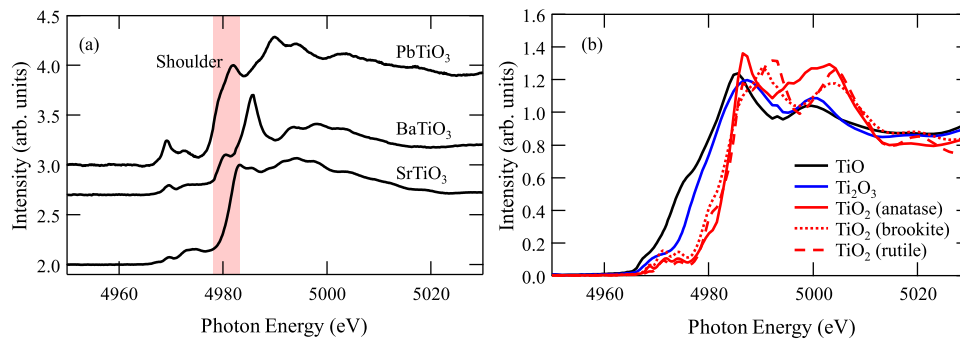
Fig. 6. Ti K-edge X-ray absorption near-edge spectra of (a) ATiO$_3$ powders (A = Pb, Ba, and Sr) and (b) TiO, Ti$_2$O$_3$, and TiO$_2$ powders.
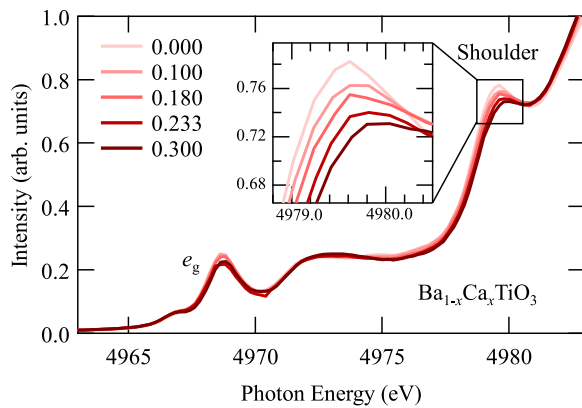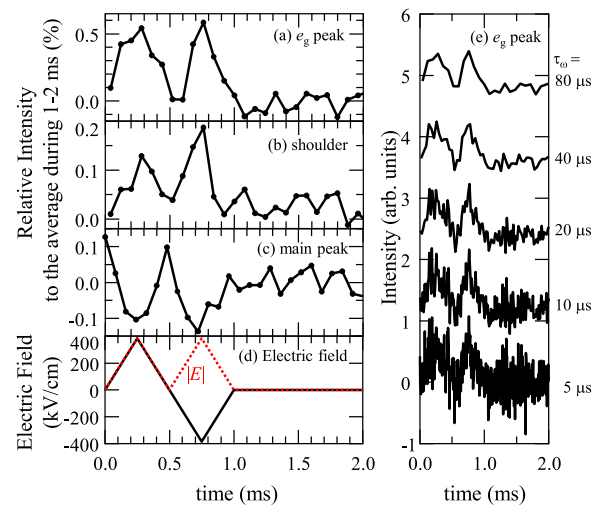

Fig. 7. Ti pre-edge X-ray absorption spectra of Ba$_{1-x}$Ca$_x$TiO$_3$ powders (x =0, 0.1, 0.18, 0.233, and 0.3).
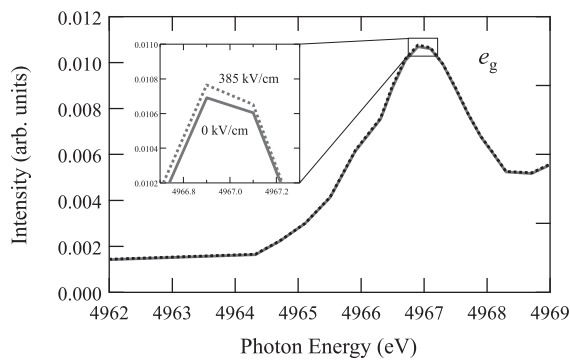
Fig. 8. Ti pre-K edge X-ray absorption spectra of BaTiO$_3$ with (solid) and without (dashed) electric fields.

Fig. 9. Time variation of the intensities of the (a) e_g peak, (b) shoulder structure, and (c) main peak under the application of (d) a triangular AC electric field. (e) Temporal variation of the e_g peak for various time windows τ_w.

tions in XAS spectra. If the valence number of Ti or its local structure changes, the chemical shifts will occur as it is seen in spectra of TiO, Ti$_2$O$_3$, and TiO$_2$, which are presented in Fig. 6(b). In our case, we did not observe any changes in the peak positions with and without electric fields. Then, we focus on the time variation of intensities.

The time variation of the area-integrated intensities of the e_g peak, shoulder structure, and main peak are presented in Fig. 9(a), (b), and (c), respectively. The integration area is set to ±1 eV around the local maxima of each spectral feature, and the integrated intensity is normalized to unity by the average intensity around an applied field of 0 V for 1–2 ms. The width of the time window (τ_w) for each plot is 80 μs. The signal to noise ratio of intensities can be estimated in the region from 1–2 ms. Intensities in this region should be constant but there is still noise left.

It is obvious that the intensities of the e_g peak and shoulder structure are synchronized with the magnitude of the applied electric field $|E|$ beyond the noise level of ∼0.05%. Intensities of both features increase as the magnitude of the applied field increases. The interaction of X-rays with the electronic states of BaTiO$_3$ is dependent not on the polarity of the electric polarization but on the magnitude of polarization; therefore, one-half period of the applied field was observed. This result confirms that not only the e_g peak but also the shoulder structure is associated with the ferroelectricity of BaTiO$_3$. In contrast, the intensity of the main peak changes in the opposite manner, i.e., its intensity decreases with increasing $|E|$. A naive interpretation of this opposite trend is the broadening of the 4p electronic states because of the reduction in the coordination symmetry of the Ti ion under the applied electric field.

To better understand the time variation of the spectral features, we studied the data presented in Fig. 9(e). In particular, this figure illustrates the time variation of the e_g-peak intensity for various τ_w. Because we detect all SDD signals using the time stamp information, it is possible to change the τ_w to any period longer than the minimum interval of the DSP-processed signals, which is typically around 0.1 μs and depends on the setting of the instrument. The time variation of the e_g-peak intensity is evident at any τ_w, even though the noise level increases as the τ_w becomes smaller. In general, the response of the electronic states to the applied electric field is instantaneous; therefore, time variation of the spectral features shows the same trend regardless of τ_w.
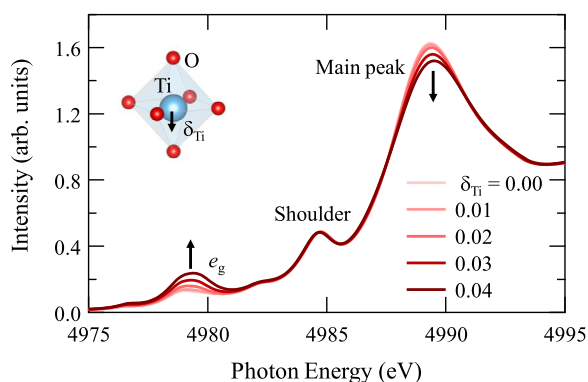
Fig. 10. Simulated Ti K-edge spectra of BaTiO$_3$ for various Ti off-center displacements (δ_{Ti}) from δ_{Ti} to 0.04 in atomic units. Calculations were performed using the FEFF 9.6 program.

To provide a theoretical background for the interpretation of the observed spectral features, the experimental spectra were compared with the simulated spectra obtained using the FEFF 9.6 program, which is based on the multiple scattering theory. [35] The simulation results are shown in Fig. 10, wherein the Ti off-center displacement (δ_{Ti}) was varied from δ_{Ti}=0 (body-center) to 0.04 in atomic units. It was assumed that larger displacements would make the spectral changes clear. As already discussed in the literature, [26] the intensity of the e_g peak increases with increasing δ_{Ti}, which reflects the enhanced Ti 3d e_g-O 2p hybridization. In contrast, the intensity of the main peak decreases in an opposite manner. The simulated results suggest that not only the effect of broadening the Ti 4p states but also the compensation for the number of unoccupied states would be a plausible reason for the observed spectral features.

In contrast to the abovementioned two features, the shoulder structure is less sensitive to the Ti off-center displacements, which clearly indicates a different physical origin for the shoulder structure. As previously mentioned, the shoulder structure was attributed to the A-site contribution in Ti as per several experimental results. One possible explanation for the A-site contribution is the Born effective charge. The Born effective charge tensor, $Z^*_{\kappa,\gamma\alpha}$, of an atom κ can be linked to the change of polarization P_γ induced by the periodic displacement $\tau_{\kappa,\alpha}$ along the α direction induced on the atom κ by an external field ε_γ: $Z^*_{\kappa,\gamma\alpha} = V\partial P_\gamma/\partial\tau_{\kappa,\alpha}$, where V is a unit cell volume. [34,36] For the simplest case, if we consider a single dipole model, the Born effective charge Z^* can be expressed by a static charge Z by using an interatomic distance u as $Z^*(u) = Z(u) + u\partial Z(u)/\partial(u)$. If $Z(u)$ changes rapidly with u, the difference between $Z(u)$ and $Z^*(u)$ becomes large. Ghosez *et al.* concluded that $Z^*_{Ba,33}$ and $Z^*_{Ti,33}$, the Born effective charge of Ba and Ti, respectively, along the ferroelectric polarization P_3, are comparable to the charge transfer between Ti and apical O along the polarization direction. Therefore, it can be stated that orbital hybridization is not restricted to Ti and O but also involves Ba, or at least, that Ba also plays an important role in the formation of the valence band.

The Born effective charge makes a major contribution to the formation of the shoulder structure; the term $u\partial Z(u)/\partial u$ is essential for the covalent character of the Ti-O bond. This term would be insensitive to the static Ti off-center displacement, as shown in the simulation in Fig. 10. Under the application of an AC electric field, not only Ti ions but also Ba ions are perturbed leading to the non-negligible enhancement of $u\partial Z(u)/\partial u$ as compared to the static environment. The intensity of the shoulder structure increases in phase with that of the e_g peak under the application of the AC field (Fig. 9). Thus, it can be speculated that the charge

transfer from the Ti 4p state to the Ba unoccupied state, e.g. the 5d state, occurs as well as the charge transfer from the Ti 3d state to the O 2p state, as concluded from the e_g peak. [26] The shoulder structure of the Ti K-edge spectrum of BaTiO$_3$ provides an electronic point of view for the dynamic piezoelectric effect of BaTiO$_3$.

Furthermore, though the A-site contribution to the ferroelectric properties of ATiO$_3$ has been observed and studied in many previous works, the polarization response under applied AC electric fields using XAS measurements provides a new insight into this, especially in terms of energetics of electronic hybridization. In this light, Ba K-edge EXAFS would provide more advanced information on the A-site contribution to the ferroelectric property of ATiO$_3$; therefore, another TR-XAS experimental study using BaTiO$_3$ under applied electric fields is currently in progress.

4. Conclusions

For the first time, Ti K-edge XAS measurements for a BaTiO$_3$ thin film were performed under the application of a triangular electric field in the TR mode. This technique enables us to detect tiny changes in spectra and observe electronic states under electric fields. Three characteristic features were studied, namely the pre-edge e_g peak, shoulder structure, and main peak. Among these three features, the responses of the first two to the electric field were in phase, whereas that of the latter was antiphase. Using model simulations, it was confirmed that Ti off-center displacements affect the increase in the e_g-peak intensity and decrease in the main peak intensity. However, it was observed that the shoulder structure was not influenced by the Ti off-center displacement. Nevertheless, it showed a dielectric response to the AC electric field that can be consistently explained from the perspective of the Born effective charge. Thus, the Ba contribution to the ferroelectric property of BaTiO$_3$ via electronic hybridization is concluded experimentally using the novel TR-XAS technique. The TR-XAS technique's utilization of the full time stamp information of the DSP is versatile for many applications; therefore, it provides a new approach for the study of the dynamical behavior of electronic states.

Declaration of Competing Interest

The authors declare that they have no known competing financial interests or personal relationships that could have appeared to influence the work reported in this paper.

Acknowledgements

References

[1] A. Devonshire, Xcvi. theory of barium titanate, The London, Edinburgh, and Dublin Philosophical Magazine and Journal of Science 40 (309) (1949) 1040–1063, doi:10.1080/14786444908561372.

[2] M. Deguchi, N. Nakajima, K. Kawakami, N. Ishimatsu, H. Maruyama, C. Moriyoshi, Y. Kuroiwa, S. Nozawa, K. Ishiji, T. Iwazumi, Luminescence mechanism of (pr, al)-doped srtio3 fine particles investigated by x-ray absorption spectroscopy, Phys. Rev. B 78 (2008) 073103, doi:10.1103/PhysRevB.78.073103.

[3] N. Nakajima, M. Deguchi, H. Maruyama, K. Ishiji, Y. Tezuka, X-ray spectroscopic study on photoluminescence properties of red phosphor SrTiO3:pr3+,al, Japanese Journal of Applied Physics 49 (9) (2010) 09ME04, doi:10.1143/jjap.49.09me04.

[4] S. Kawakami, N. Nakajima, T. Takigawa, M. Nakatake, H. Maruyama, Y. Tezuka, T. Iwazumi, Uv-induced change in the electronic structure of srtio3 at low temperature probed by resonant x-ray emission spectroscopy, Journal of the Physical Society of Japan 82 (5) (2013) 053701, doi:10.7566/JPSJ.82.053701.

[5] S. Kawakami, N. Nakajima, M. Nakatake, N. Kawamura, M. Mizumaki, H. Maruyama, Mechanism of intrinsic dipole moment induction in quantum paraelectric SrTiO3, Japanese Journal of Applied Physics 54 (10S) (2015) 10NC03, doi:10.7567/jjap.54.10nc03.

[6] C. Lu, C. Temba, N. Nakajima, S. Kawakami, N. Ishimatsu, H. Maruyama, Isotropic shrinkage of the oxygen octahedron in SrTiO3 under uniaxial pressure, Journal of Physics: Condensed Matter 29 (39) (2017) 395502, doi:10.1088/1361-648x/aa7ec6.

[7] B. Ravel, E. Stern, Local disorder and near edge structure in titanate perovskites, Physica B: Condensed Matter 208-209 (1995) 316–318, doi:10.1016/0921-4526(94)00686-P. Proceedings of the 8th International Conference on X-ray Absorption Fine Structure

[8] B. Ravel, E.A. Stern, R.I. Vedrinskii, V. Kraizman, Local structure and the phase transitions of batio3, Ferroelectrics 206 (1) (1998) 407–430, doi:10.1080/00150199808009173.

[9] A. Bootchanont, J. Jutimoosik, S. Chandarak, M. Unruan, P. Kidkhunthod, W. Klysubun, S. Rujirawat, R. Yimnirun, R. Guo, A. Bhalla, Synchrotron x-ray absorption spectroscopy study of local structure transformation behavior in perovskite ba(ti,zr)o3 system, Journal of Alloys and Compounds 616 (2014) 430–435, doi:10.1016/j.jallcom.2014.07.175.

[10] P. Phaktapha, J. Jutimoosik, A. Bootchanont, P. Kidkhunthod, S. Rujirawat, R. Yimnirun, Temperature dependent local structure in batio3 single crystal, Integrated Ferroelectrics 177 (1) (2017) 74–78, doi:10.1080/10584587.2017.1285183.

[11] A. Yoshiasa, G. Kitahara, T. Tobase, T. Hiratoko, H. Hongu, T. Nakatani, K.-i. Murai, Determination of feffo- and antiferroelectricity using the temperature dependence of the pre-edge features in the xanes spectra: Xanes study of tetragonal and cubic atio3 (a = sr, ba, and pb) and pbzro3, physica status solidi (b) 255 (11) (2018) 1800050, doi:10.1002/pssb.201800050.

[12] R.H. Buttner, E.N. Maslen, Structural parameters and electron difference density in batio3, Acta Crystallographica Section B 48 (6) (1992) 764–769, doi:10.1107/S010876819200510X.

[13] R.H. Mitchell, A.R. Chakhmouradian, P.M. Woodward, Crystal chemistry of perovskite-type compounds in the tausonite-loparite series, (sr1-2xnaxlax)tio3, Physics and Chemistry of Minerals 27 (8) (2000) 583–589, doi:10.1007/s002690000103.

[14] A.M. Glazer, S.A. Mabud, Powder profile refinement of lead zirconate titanate at several temperatures. ii. pure pbtio3, Acta Crystallographica Section B 34 (4) (1978) 1065–1070, doi:10.1107/S0567740878004938.

[15] R.E. Cohen, H. Krakauer, Electronic structure studies of the differences in ferroelectric behavior of batio3 and pbtio3, Ferroelectrics 136 (1) (1992) 65–83, doi:10.1080/00150199208016067.

[16] Y. Kuroiwa, S. Aoyagi, A. Sawada, J. Harada, E. Nishibori, M. Takata, M. Sakata, Evidence for pb-o covalency in tetragonal pbtio3, Phys. Rev. Lett. 87 (2001) 217601, doi:10.1103/PhysRevLett.87.217601.

[17] A. Anspoks, C. Marini, T. Miyanaga, B. Joseph, A. Kuzmin, J. Purans, J. Timoshenko, A. Bussmann-Holder, Local structure of a-atom in abo3 perovskites studies by rmc-exafs, Radiation Physics and Chemistry (2018).

[18] C. Moriyoshi, S. Hiramoto, H. Ohkubo, Y. Kuroiwa, H. Osawa, K. Sugimoto, S. Kimura, M. Takata, Y. Kitanaka, Y. Noguchi, M. Miyayama, Synchrotron radiation study on time-resolved tetragonal lattice strain of batio3 under electric field, Japanese Journal of Applied Physics 50 (9) (2011) 09NE05, doi:10.1143/jjap.50.09ne05.

[19] R. Tazaki, D. Fu, M. Itoh, M. Daimon, S. ya Koshihara, Lattice distortion under an electric field in BaTiO3 piezoelectric single crystal, Journal of Physics: Condensed Matter 21 (21) (2009) 215903, doi:10.1088/0953-8984/21/21/215903.

[20] K.J. Choi, M. Biegalski, Y.L. Li, A. Sharan, J. Schubert, R. Uecker, P. Reiche, Y.B. Chen, X.Q. Pan, V. Gopalan, L.-Q. Chen, D.G. Schlom, C.B. Eom, Enhancement of ferroelectricity in strained batio3 thin films, Science 306 (5698) (2004) 1005–1009, doi:10.1126/science.1103218.

[21] M. Tyunina, O. Pacherova, J. Peräntie, M. Savinov, M. Jelinek, H. Jantunen, A. Dejneka, Perovskite ferroelectric tuned by thermal strain, Scientific reports 9 (1) (2019) 3677, doi:10.1038/s41598-019-40260-y.

[22] N. Setter, D. Damjanovic, L. Eng, G. Fox, S. Gevorgian, S. Hong, A. Kingon, H. Kohlstedt, N.Y. Park, G.B. Stephenson, I. Stolitchnov, A.K. Tagantsev, D.V. Taylor, T. Yamada, S. Streiffer, Ferroelectric thin films: Review of materials, properties, and applications, Journal of Applied Physics 100 (5) (2006) 051606, doi:10.1063/1.2336999.

[23] J. Shin, A. Goyal, S. Jesse, D.H. Kim, Single-crystal-like, c-axis oriented batio3 thin films with high-performance on flexible metal templates for ferroelectric applications, Applied Physics Letters 94 (25) (2009) 252903, doi:10.1063/1.3158955.

[24] G. Arlt, H. Neumann, Internal bias in ferroelectric ceramics: Origin and time dependence, Ferroelectrics 87 (1) (1988) 109–120, doi:10.1080/00150198808201374.

[25] Z. Luo, S. Pojprapai, J. Glaum, M. Hoffman, Electrical fatigue-induced cracking in lead zirconate titanate piezoelectric ceramic and its influence quantitatively analyzed by refatigue method, Journal of the American Ceramic Society 95 (8) (2012) 2593–2600, doi:10.1111/j.1551-2916.2012.05232.x.

[26] R.V. Vedrinskii, V.L. Kraizman, A.A. Novakovich, P.V. Demekhin, S.V. Urazhdin, Pre-edge fine structure of the 3d atom k x-ray absorption spectra and quantitative atomic structure determinations for ferroelectric perovskite structure crystals, Journal of Physics: Condensed Matter 10 (42) (1998) 9561–9580, doi:10.1088/0953-8984/10/42/021.

[27] F. De Groot, G. Vankó, P. Glatzel, The 1s x-ray absorption pre-edge structures in transition metal oxides, Journal of physics. Condensed matter : an Institute of Physics journal 21 (2009) 104207, doi:10.1088/0953-8984/21/10/104207.

[28] A. Anspoks, D. Bocharov, J. Purans, F. Rocca, A. Sarakovskis, V. Trepakov, A. Dejneka, M. Itoh, Local structure studies of SrTi16o3 and SrTi18o3, Physica Scripta 89 (4) (2014) 044002, doi:10.1088/0031-8949/89/04/044002.

[29] P. Blanchard, A. Grosvenor, Investigating the local structure of b -site cations in (1- x)batio 3 – x bisco 3 and (1- x)pbtio 3 – x bisco 3 using x-ray absorption spectroscopy, Solid State Sciences 79 (2018), doi:10.1016/j.solidstatesciences.2018.02.018.

[30] D. Fu, M. Itoh, S. Koshihara, Invariant lattice strain and polarization in batio3-catio3 ferroelectric alloys, Journal of Physics: Condensed Matter 22 (5) (2010) 052204, doi:10.1088/0953-8984/22/5/052204.

[31] D. Fu, M. Itoh, S.-y. Koshihara, T. Kosugi, S. Tsuneyuki, Anomalous phase diagram of ferroelectric (ba,ca)tio3 single crystals with giant electromechanical response, Phys. Rev. Lett. 100 (2008) 227601, doi:10.1103/PhysRevLett.100.227601.

[32] I. Levin, E. Cockayne, V. Krayzman, J.C. Woicik, S. Lee, C.A. Randall, Local structure of ba(ti,zr)o3 perovskite-like solid solutions and its relation to the band-gap behavior, Phys. Rev. B 83 (2011) 094122, doi:10.1103/PhysRevB.83.094122.

[33] A. Bootchanont, J. Jutimoosik, S. Chandarak, M. Unruan, S. Rujirawat, R. Yimnirun, R. Guo, A. Bhalla, Investigation of local structure in batio3-bazro3 system by synchrotron x-ray absorption spectroscopy, Ceramics International 39 (2013) S579–S582, doi:10.1016/j.ceramint.2012.10.139. The 8th Asian Meeting on Electroceramics (AMEC-8)

[34] P. Ghosez, X. Gonze, P. Lambin, J.-P. Michenaud, Born effective charges of barium titanate: Band-by-band decomposition and sensitivity to structural features, Phys. Rev. B 51 (1995) 6765–6768, doi:10.1103/PhysRevB.51.6765.

[35] J.J. Rehr, J.J. Kas, F.D. Vila, M.P. Prange, K. Jorissen, Parameter-free calculations of x-ray spectra with feff9, Phys. Chem. Chem. Phys. 12 (2010) 5503–5513, doi:10.1039/B926434E.

[36] P.R. Tulip, Dielectric and lattice dynamical properties of molecular crystals via density functional perturbation theory: implementation within a first principles code, Durham University, 2004 Ph. d thesis.